Available online at www.sciencedirect.com
ScienceDirect
Journal of Sound and Vibration 321 (2009) 662–679
JOURNAL OF SOUND AND VIBRATION
www.elsevier.com/locate/jsvi

Numerical study of time domain analogy applied to noise prediction from rotating blades

D. Fedala[a,*], S. Kouidri[b], R. Rey[a]

[a]*Laboratoire d'Energétique et de Mécanique des Fluides Interne, Ecole Nationale Supérieure d'Arts et Métiers, 151, bd. de l'Hôpital, 75013 Paris, France*

[b]*Laboratoire d'Informatique pour la Mécanique et les Sciences de l'Ingénieur LIMSI-CNRS Bâtiments 508 et 502bis, Université de Paris-Sud, 91403 Orsay, France*

Received 29 October 2007; received in revised form 12 October 2008; accepted 15 October 2008
Handling Editor: C.L. Morfey
Available online 30 November 2008

Abstract

Aeroacoustic formulations in time domain are frequently used to model the aerodynamic sound of airfoils, the time data being more accessible. The formulation 1A developed by Farassat, an integral solution of the Ffowcs Williams and Hawkings equation, holds great interest because of its ability to handle surfaces in arbitrary motion. The aim of this work is to study the numerical sensitivity of this model to specified parameters used in the calculation. The numerical algorithms, spatial and time discretizations, and approximations used for far-field acoustic simulation are presented. An approach of quantifying of the numerical errors resulting from implementation of formulation 1A is carried out based on Isom's and Tam's test cases.

A helicopter blade airfoil, as defined by Farassat to investigate Isom's case, is used in this work. According to Isom, the acoustic response of a dipole source with a constant aerodynamic load, $\rho_0 c_0^2$, is equal to the thickness noise contribution. Discrepancies are observed when the two contributions are computed numerically. In this work, variations of these errors, which depend on the temporal resolution, Mach number, source–observer distance, and interpolation algorithm type, are investigated. The results show that the spline interpolating algorithm gives the minimum error. The analysis is then extended to Tam's test case. Tam's test case has the advantage of providing an analytical solution for the first harmonic of the noise produced by a specific force distribution.

1. Introduction

Noise reduction is one of the challenges that the transportation industry has to face because of the client demands as well as increasing legal restrictions. Today, accurate prediction of the aerodynamic noise is playing a major role in the development of new noise reducing concepts. A powerful approach consists of coupling advanced aerodynamic simulations with the aeroacoustic analogy. This technique is commonly used to predict noise radiated by propellers, helicopter rotors, and fans. The aerodynamic simulation has to

*Corresponding author. Tel.: +330 1 44 24 64 12; fax: +330 1 44 24 63 98.
E-mail address: djaafer.fedala@paris.ensam.fr (D. Fedala).

0022-460X/$ - see front matter © 2008 Elsevier Ltd. All rights reserved.
doi:10.1016/j.jsv.2008.10.015

Nomenclature

c_0	ambient sound speed
$\mathrm{d}S$	element of the control surface
$D(\theta)$	Tam's directivity in spherical coordinates
$f(\mathbf{x},t)=0$	function that describes the source surface
F_x, F_r, F_φ	Tam's forces in cylindrical coordinates
$H(f)$	Heaviside function
$J_m(\ )$	the mth-order Bessel function
L_i	components of local force that acts on the fluid, $Li=\lfloor(p-p_0)\delta_{ij}-\tau_{ij}+\rho u_i(u_j-v_i)\rfloor n_j$
$\dot{L}_r$	$\frac{\partial L_i}{\partial\tau}\frac{r_i}{r}$
$\mathbf{M}$	local Mach number vector of source with respect to a frame fixed to the undisturbed medium, with components M_i
$\dot{\mathbf{M}}$	$\partial M_i/\partial\tau$
M_n	Mach number in direction normal to the surface, $M_i n_i$
M_r	Mach number of source in radiation direction, $M_i\hat{r}_i$
$\dot{M}_r$	$\dot{M}_i\hat{r}_i$
$\mathbf{n}$	unit outward normal vector to the surface, with components n_i
N_t	number of time steps per period
$\tilde{p}$	far-field acoustic pressure
$\tilde{p}_L$	loading noise component
$\tilde{p}_T$	thickness noise component
P_{ij}	compressive stress tensor components
r	source–observer distance, $r=\lvert\mathbf{x}-\mathbf{y}\rvert$
$\hat{\mathbf{r}}$	unit vector in the radiation direction, with components $\hat{r}_i$
t	observer time
t_n	the nth time step
T	blade passage time
T_{ij}	Lighthill stress tensor, $\rho u_i u_j+P_{ij}-c_0^2\rho'\delta_{ij}$
u_i	components of local fluid velocity
v_i	components of control surface velocity
v_n	normal velocity of source surface, $v_i n_i$
$v_{\dot{n}}$	$v_i\dot{n}_i$
$\dot{v}_n$	$\dot{v}_i n_i$
$\mathbf{x}$	observer position vector, with components x_i
$(x,\ r,\ \varphi)$	cylindrical coordinates for Tam's test case
$\mathbf{y}$	source position vector, with components y_i
$\delta(f)$	Dirac function
δ_{ij}	Kronecker delta
λ_{mN}	the Nth root of J'_m; i.e., $J'_m(\lambda_{mN})=0$
θ	the angle defined by the rotation axis and the source–observer direction
Ω	rotor angular velocity
ρ_0	density of the medium at rest
τ	source time (retarded-time)
τ_{ij}	viscosity stress tensor components.

Indices:

$\dot{[\,]}$	the dotted variables denote retarded temporal derivatives
$[\,]_r$	index denotes projection onto the source–observer direction
$[\,]_M$	index denotes projection on the Mach number vector

accurately determine the unsteady loading on the blades, which are used in Ffowcs Williams and Hawkings (FW&H) integral formulations. Noise sources are only computed around the surface. Then, far-field acoustic pressure can be calculated by the evaluation of integrals.

Significant theoretical and computational advancements have been achieved with the development of the time domain integral formulations. Today, almost all deterministic rotor noise predictions are based on time-domain integral formulations of the FW&H equation. Formulation 1A, an integral solution of the FW&H equation developed by Farassat [1], holds great interest because of its ability to handle surfaces in arbitrary motion. Di Francescantonio [2] proposed a new boundary integral formulation, which does not require the non-penetration condition nor the calculation of the surface pressure normal derivative. Casalino [3] introduced the advanced time approach in the retarded-time formulation 1A of Farassat. Then, the algorithms are more efficient because no iterative solutions of the retarded-time equation need to be performed. Ghorbaniasl and Hirsch [4] presented a series of test cases which are helping to validate the numerical implementation of the Farassat's formulation 1A.

Although progresses has been reported in developing this approach, the results are still very sensitive to the algorithms, spatial and time discretizations, and approximations used for far-field acoustic simulation. Thus, quantifying the numerical errors resulting from implementation of formulation 1A is essential for rigorous noise predictions. In addition, computational codes must be verified and validated by means of well-known test cases. The verification can be ideally carried out by comparing the computations to analytical solutions; the numerical errors are calculated through the discrepancies between the numerical and analytical solutions.

The new aspect of this work is a contribution to improve the numerical method accuracy of aeroacoustic predictions. For this, numerical errors resulting from implementation of formulation 1A are quantified. The computational and physical parameters, such as the tip Mach number, position of the observer, temporal resolution, and accuracy of the numerical derivation, are investigated based on an efficient test case: Isom's test [5]. According to Isom, the acoustic response of a moving dipole source with a constant aerodynamic load, $\rho_0 c_0^2$, is equal to the thickness noise contribution. Hence, Isom gave a consistency test to validate aeroacoustic calculation codes. However, even if an integral formulation is well implemented, discrepancies are observed between Isom's computed result and thickness noise. Variations of these errors which depend on the aforementioned computational parameters are investigated. The analysis is then completed with Tam's test benchmark [6,7]. Tam's test case has the advantage of providing an analytical solution for the first harmonic of the produced noise by specific force distribution.

2. Formulation 1A: numerical implementation

In this part, development of the Ffowcs Williams and Hawkings equation [8] is carried out. The acoustic solver is based on the integral retarded-time FW&H formulation 1A with permeable surfaces of Di Francescantonio [2] and Brentner and Farassat [1,9]. The interest of this formulation lies in the fact that time derivative of the integral terms of FW&H has been eliminated. Moreover, the evaluation of the noise can be done even if the observer is moving. The thickness and the loading noise of a surface in arbitrary motion are given as

$$\begin{cases} \tilde{p}_T(\mathbf{x},t) = \tilde{p}_{T1}(\mathbf{x},t) + \tilde{p}_{T2}(\mathbf{x},t) \\ \tilde{p}_L(\mathbf{x},t) = \tilde{p}_{L1}(\mathbf{x},t) + \tilde{p}_{L2}(\mathbf{x},t) + \tilde{p}_{L3}(\mathbf{x},t) \end{cases} \tag{1}$$

so

$$\tilde{p}(\mathbf{x},t) = \tilde{p}_T(\mathbf{x},t) + \tilde{p}_L(\mathbf{x},t) \tag{2}$$

where

$$4\pi\tilde{p}_{T1}(\mathbf{x},t) = \iint_{f(y,\tau)=0} \left[\frac{\rho_0(\dot{U}_n + U_{\dot{n}})}{rD^2}\right]_{\tau=t-r/c_0} \mathrm{d}S \tag{3}$$

$$4\pi\tilde{p}_{T2}(\mathbf{x},t) = \iint_{f(y,\,\tau)} \left[\frac{\rho_0 U_n(r_i\dot{M}_i + c_0(M_r - M^2))}{r^2D^3}\right]_{\tau=t-r/c_0} \mathrm{d}S \tag{4}$$

and

$$4\pi\tilde{p}_{L1}(\mathbf{x},t) = \frac{1}{c_0}\iint_{f(y,\tau)=0} \left[\frac{\dot{L}_r}{rD^2}\right]_{\tau=t-r/c_0} \mathrm{d}S \tag{5}$$

$$4\pi\tilde{p}_{L2}(\mathbf{x},t) = \iint_{f(y,\tau)=0} \left[\frac{L_r - L_M}{r^2D^2}\right]_{\tau=t-r/c_0} \mathrm{d}S \tag{6}$$

$$4\pi\tilde{p}_{L3}(\mathbf{x},t) = \frac{1}{c_0}\iint_{f(y,\tau)=0} \left[\frac{L_r(r\dot{M}_r + c_0(M_r - M^2))}{r^2D^3}\right]_{\tau=t-r/c_0} \mathrm{d}S \tag{7}$$

$\tilde{p}$ is the acoustic pressure, $\mathbf{x}$ the observer position and $\mathbf{y}$ the source position so $r = |\mathbf{x}-\mathbf{y}|$ is the source–observer distance, $D = 1-M_r$ the Doppler factor, $\mathbf{L}$ the aerodynamic pressure forces with $L_i = \lfloor (p-p_0)\delta_{ij} - \tau_{ij} + \rho u_i(u_j - v_j)\rfloor n_j$, τ_{ij} the viscosity stress tensor and δ_{ij} Kronecker symbol. ρ_0 and c_0 are, respectively, the density of the fluid and the sound speed in a medium at rest. v_i is the velocity of the control surface and u_i represents the fluid velocity so $U_i = \rho u_i/\rho_0 + (1-\rho/\rho_0)v_i$. When the control surface is solid, the relative velocity $(u_i-v_i) = 0$ and U_i is reduced to $U_i = v_i$. It is important to point out that the terms between the brackets of Eqs. (3)–(7) are evaluated at retarded time. The retarded-time integrals have the following general form:

$$4\pi\phi(\mathbf{x},t) = \iint\limits_{f(y,\tau)=0} \left[\frac{Q}{r^{N1}|1-M_r|^{N2}}\right]_{\tau=t-r/c_0} \mathrm{d}S \tag{8}$$

where N_1 and N_2 are integers. These integrals are approximated by mid-panel-quadrature algorithm. The source surface is divided into N panels. The values of the Q's are approximated at panel centroids, with mc indices and $\mathbf{y}_{mc}$ coordinates.

The retarded integrals are then calculated as

$$4\pi\phi(\mathbf{x},t) \approx \sum_{mc=1}^{N} \frac{Q(\mathbf{y}_{mc},\ t-r_{mc}/c_0)}{r_{mc}^{N1}|1-M_r|_{mc}^{N2}} \Delta S_{mc} \tag{9}$$

Integrals are evaluated with the source time regarded as the primary time (i.e., dominant). The source time for a panel is chosen and determines when the signal will reach the observer. The second then the fourth-order equidistant derivations, described in Appendix A, are used in this work for the calculation of $\dot{L}_i$ based on the inputs of $p(t)$. If the observer is static, then the expression of reception time is given as

$$t = \tau + \frac{r(\tau)}{c_0} \tag{10}$$

where τ is the emission time. For a moving observer, an expression of the advanced time has been given by Casalino [3]. The acoustic signal is the summation of all computed values of disturbances emitted by the sources at different retarded times and reaching the observer at a unique observer time. Thus, an interpolation of the acoustic pressure at reception time is performed so that the contributions from all source panels can be summed at the same observer times. The interpolation is carried out with linear, spline and piecewise cubic Hermite interpolating polynomial algorithms available in Matlab 6.

3. Isom test case

Firstly, the Isom test [5] is reviewed. It has been shown that if a constant aerodynamic load, $\rho_0 c_0^2$, is applied over a moving surface, the generated thickness noise and loading noise must be equal. This assumption can be demonstrated by applying the wave operator, $\Box^2 = \left((1/c_0^2)(\partial^2/\partial t^2) - \nabla^2\right)$, to the generalized function $\rho_0 c_0^2[1-H(f)]$ that is always equal to zero out of the surface defined by $f(\mathbf{x},t) = 0$. Then, the mathematical form of the thickness noise and the loading noise are recognized as the left and right sides of Eq. (11), respectively:

$$\frac{\partial}{\partial t}[\rho_0 v_n \delta(f)] = -\frac{\partial}{\partial x_i}[\rho_0 c_0^2 n_i \delta(f)] \tag{11}$$

A more complete derivation can be found in Refs. [5,10,11]. This analytical result is not always exact when applied numerically due to the differences of robustness in the integration of the two noises. This difference is affected by several geometrical and physical parameters of which the influence has not been well studied.

A conventional rotor has been defined for use in Isom's test case. The same helicopter rotor, as defined by Farassat et al. [11] to study Isom's case, is used in this work. It is composed of two blades, Fig. 1(a), of 4 m spanwise length for an external diameter of 10 m. The blades are symmetrical biconvex airfoils with a 10 percent thickness ratio (a NACA0010 profile is used). The main chord is equal to 0.4 m.

In their first calculations, Farassat et al. [12] did not take into account the tips and the inner faces of the blades and the results did not agree with the theory. Subsequently, they found that the blade tip is an effective noise generation area when Isom's thickness noise formulae were studied [13]. This being corrected, a

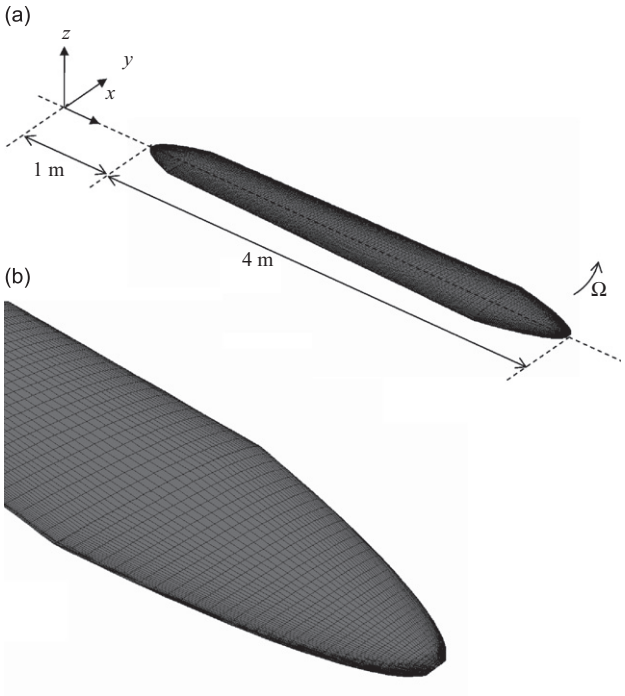

Fig. 1. (a) Blade geometry. (b) Close-up of the blade tip showing the thickness ratio decreases at the extremities of the blade.

non-negligible discrepancy remained especially at low tip Mach numbers. Their first idea was to decrease the thickness ratio at the extremities of the blade. Fig. 1(b) includes an expanded version of the end of the blade, which shows this decreasing thickness. Thus, the quality of the results is improved. The last modification, adapted by Ghorbaniasl and Hirsch [4], consists of refining the grid at the inner and outer radii of the blade. Once these improvements are performed, the result is excellent for the specified configuration. In these previous studies, Isom's thickness noise formula was used as a verification test case and the evolution of the errors which depend on the computational and physical parameters were not presented. Therefore, there is a need to study their effect on the numerical accuracy of the results.

Firstly, the results obtained with the code developed during this study for the blade shown in Fig. 1 and tip Mach numbers of 0.4 and 0.8 are presented in Fig. 2. The observer is located in the rotation plane at 50 m away from the rotation axis. The temporal resolution consists of 512 time steps per period. The interpolation of acoustic pressure signals is based on the spline algorithm. The acoustic pressures are non-dimensionalized with respect to $\rho_0 c_0^2$. A good agreement is noticed between the Isom and thickness noise showing that the numerical implementation is correct.

3.1. Error definition

In order to compare the results obtained when parameters are varied, an accurate definition of the error is required. This definition must allow a study of the Mach number, time step, and source–observer distance effects. For Isom's test case, two sets of values must be compared, $\tilde{p}_L$ and $\tilde{p}_T$, whereas, for Tam's benchmark, the comparison is conducted for analytical and numerical solutions. An error metric is defined as the maximum value of the difference between Isom's and thickness noise during one time period:

$$E_m = \max_{t=t_0}^{t=T}(|\tilde{p}_T(t) - \tilde{p}_L(t)|) \tag{12}$$

When the results are varying over a wide range, a relative error is also investigated. In case of comparison with an analytical solution, definition of the relative error can be written as $E_r(t_n) = |\tilde{p}_{\text{numerical}} - \tilde{p}_{\text{analytical}}|/|\tilde{p}_{\text{analytical}}|$. However, in Isom's test case, both of dipole and thickness noises are computed numerically.

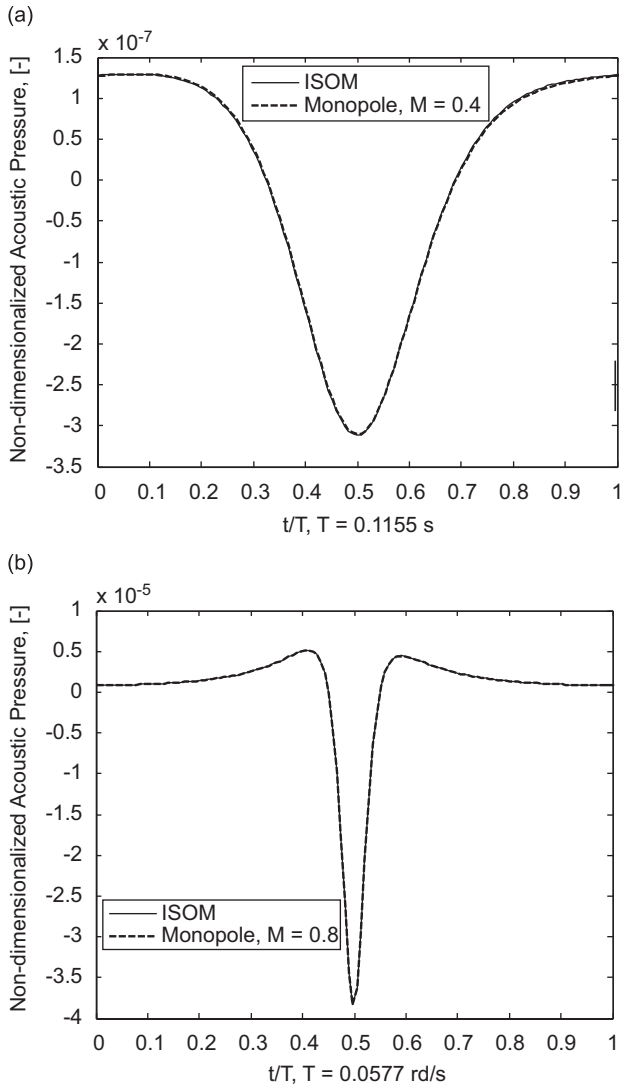

Fig. 2. Acoustic pressure signatures for a two-bladed rotor, (a) tip Mach number 0.4, (b) tip Mach number 0.8.

Alternatively, the maximum level is $\max(|\tilde{p}_T(t_n)|; |\tilde{p}_L(t_n)|)$ taken as the reference value, and definition of E_r for comparison of loading and thickness noises at each time step is given as

$$E_r(t_n) = \frac{|\tilde{p}_T(t_n) - \tilde{p}_L(t_n)|}{\max(|\tilde{p}_T(t_n)|; |\tilde{p}_L(t_n)|)} \tag{13}$$

The relative error, E_r, then takes into account the scale (magnitude). This definition allows error varying from 0 to 1. In order to evaluate the discrepancy between two curves, the error considered is the arithmetical mean of the time relative errors:

$$\overline{E}_r = \frac{1}{N_t} \sum_{t=t_0}^{T} E_r(t_n) \tag{14}$$

It is important to point out that the aerodynamic loading is constant, equal to $\rho_0 c_0^2$, in Eqs. (12)–(14) so that $\tilde{p}_L = \tilde{p}_{ISOM}$, and the errors identify differences between the Isom and thickness noise. These differences

quantify numerical errors resulting from numerical implementation of formulation 1A. Ideally, they should be equal to zero.

3.2. Mach number

As noticed by Brentner and Farassat [11], for subsonic motions, the discrepancy between computed Isom's noise and thickness noise, which are theoretically equal, increases when Mach number is decreasing. A good illustration is given in Fig. 3 for 0.2 tip Mach number. The parameters used are the same as those in computation of the results for 0.4 and 0.8 Mach numbers (Fig. 2).

In order to study the sensitivity of the model to the tip Mach number, the same configuration is kept and only the tip Mach number is varied from 0.1 to 0.9. The non-dimensional error metric, as shown in Fig. 4(a), is increasing with the tip Mach number. Here, the error metric is not representative of the discrepancies; it is predictable that the metric error varies in the same way as for the acoustic pressure amplitudes, which are more important for higher Mach numbers. The evolution of the relative error as a function of the Mach number is then represented in Fig. 4(b). The mean relative error decreases when the Mach number is increasing. This result suggests that the mesh grid has to be refined near the regions moving at low Mach number, i.e., near the inner radius. Computation accuracy at low Mach numbers is of practical interest for the loading noise prediction. Actually, these errors are also representative of the computation accuracy of loading noise since the same algorithms are used in the computation of both noises.

3.3. Temporal resolution, interpolation algorithm types and order of the derivation

In this section, the previous geometry is kept with the same mesh grid, the observer is in the rotation plane, and the number of time steps per one rotation period is varied. The linear, spline and piecewise cubic Hermite interpolating polynomial algorithms are compared. For each case, two differentiation algorithms are used in the computation of $\dot{\mathbf{L}}$: second-order (R2) and fourth-order equidistant derivations scheme (R4). The error metric, E_m, as a function of the number of time steps per period, for 0.1, 0.2, 0.4, 0.6 and 0.8 tip Mach numbers is presented in Fig. 5. As expected, these errors decrease when the temporal resolution is refined. For all the investigated tip Mach numbers, the results are very sensitive to the interpolation algorithm type. The spline algorithm gives the best results for all tip Mach numbers. The spline method is known to produce a smoother result, i.e., is continuous if the data are smooth which is actually our case. As expected, from Fig. 5(e), the linear interpolation is less stable and gives the worst results. The cubic method is known to preserve

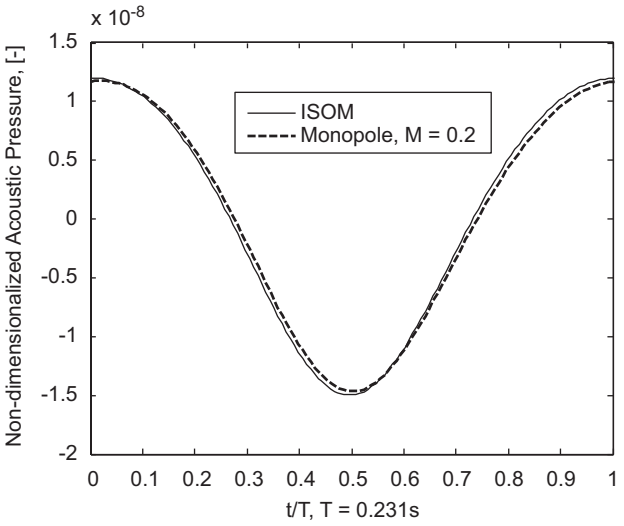

Fig. 3. Acoustic pressure signatures for a two-bladed rotor, tip Mach number 0.2.

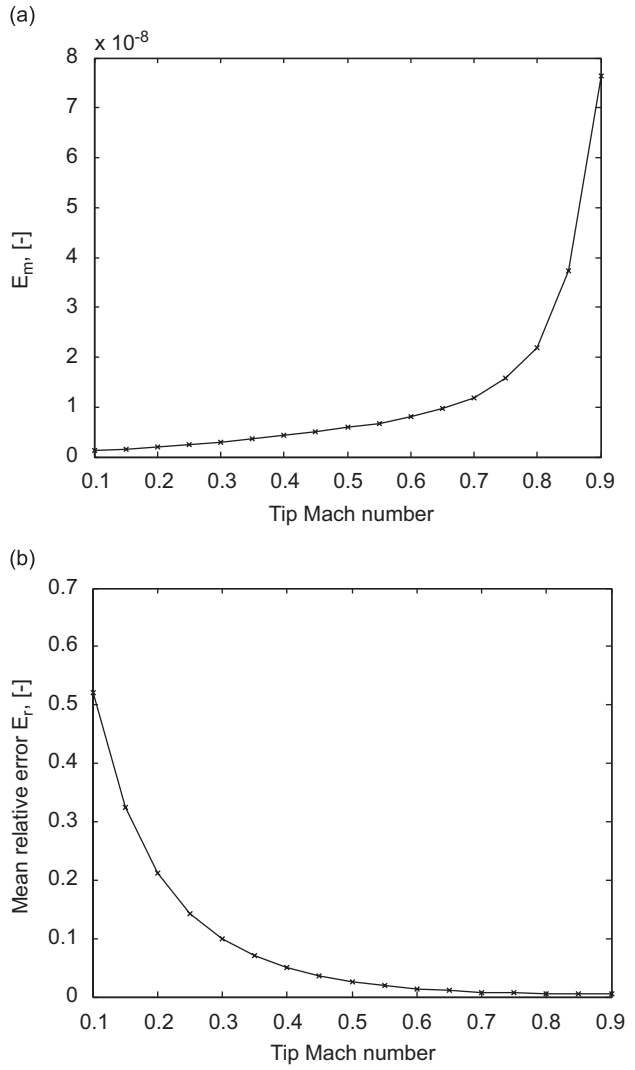

Fig. 4. Numerical errors as a function of tip Mach number, (a) error metric E_m, (b) mean relative error $\overline{E}_r$.

monotonicity and the shape of the data. For all cases, the fourth-order derivation gives better results particularly for the spline interpolation. For the configuration presented, 512 time steps per period are sufficient to give a minimal error. This value is used for the following computations with the spline algorithm for interpolation of acoustic pressure signals and the fourth-order equidistant derivation scheme.

The non-dimensional computation time as a function of the number of time steps per period is represented for the different interpolating algorithms in Fig. 6. The time resource needed for 2024 time steps per period with the spline algorithm is taken as the reference value. The computation time is directly proportional to temporal resolution. For the linear and the piecewise cubic Hermite interpolating algorithms, the cost is respectively around 91 and 95 percent of the computation time needed for the spline algorithm.

3.4. Source–observer distance

The parameter considered in this section is the source–observer distance. Even if, theoretically, the formulation F1A is adequate to predict aeroacoustic noise in near-field domain, as noticed in Brentner and Farassat [9], the numerical results are sensitive to source–observer distance.

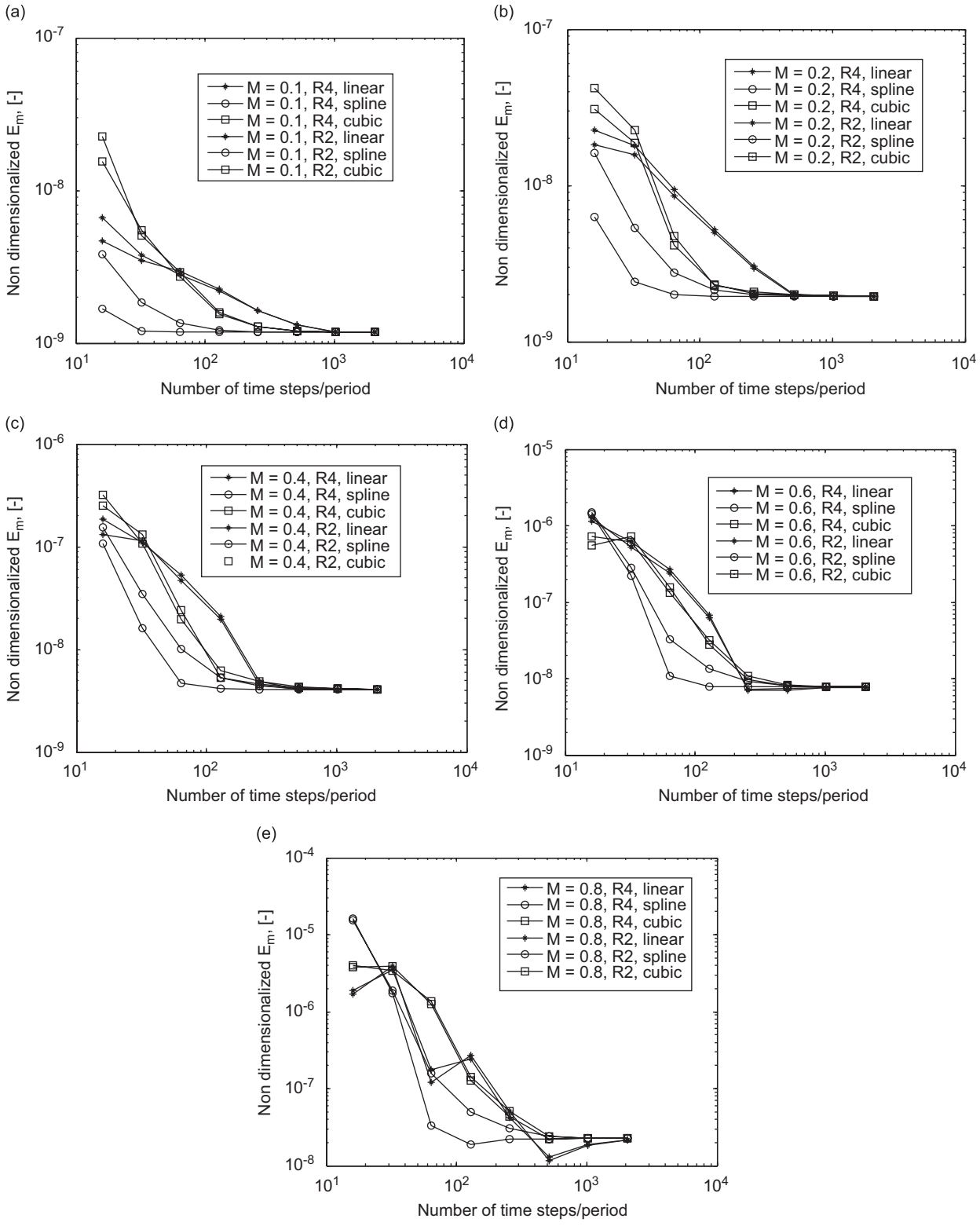

Fig. 5. Numerical errors as a function of number of time steps per period for different interpolation algorithm types, orders of the derivation and tip Mach numbers, (a) $M = 0.1$, (b) $M = 0.2$, (c) $M = 0.4$, (d) $M = 0.6$, (e) $M = 0.8$.

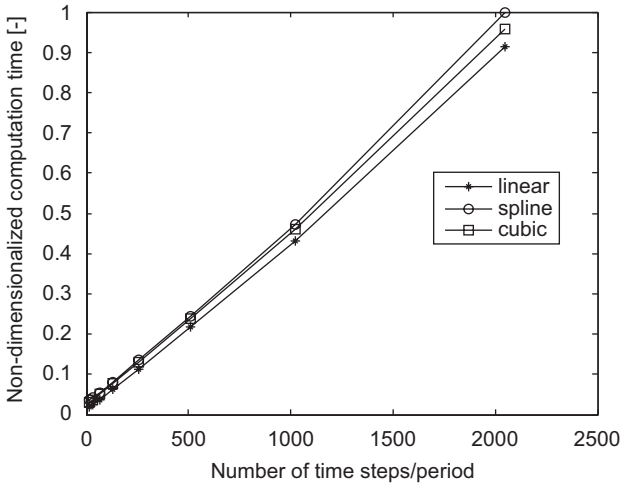

Fig. 6. Computation time as a function of the number of time steps per period.

The error metric dependence on the source–observer distance is represented in Fig. 7(a). The distances are non-dimensionalized with respect to the blade span (4 m). The discrepancies decrease when the observer is in the far field. When the mean relative error $\overline{E}_r$ is considered, as shown in Fig. 7(b), although a minimum is noticed around 250 m, the discrepancy between loading noise and thickness noise is relatively constant in relative value staying between 0.53 and 0.57 percent. In other terms, the integrals in far-field domain $(1/r)$ and near-field domain $(1/r^2)$ are estimated with the same accuracy. Source–observer distance is not a source of error and the numerical scheme presented describes far-field domain as well as near-field noise generation confirming the ability to predict the aeroacoustic noise in near-field domain.

3.5. Directivity

In order to study the directivity, the observer is located at 50 m away from the rotation center and the angle defined by observer position vector and the rotation plane is varied. An angle of 0° corresponds to the observer position at the rotation plane. The tip Mach number is fixed at 0.8. The number of time steps per rotation period is 512. Figs. 8(a) and (b) show respectively the non-dimensional and the levels in dB of the maxima of $|\tilde{p}_T|$ and $|\tilde{p}_L|$ over one period depending on the rotation angle. The directivity feature shows a dipole character. Acoustic pressures found are maxima in the rotation plane. On the other hand, they are minima along the rotation axis. On the rotation axis, the tangential aerodynamic forces, are not responsible for noise emission since the source terms L_r are null for this force components (the tangential forces are perpendicular to source–observer vector **r**). Only the axial forces can generate noise on the rotation axis.

The error metric as shown on Fig. 9(a) is more significant out of the rotation plane. This result suggests that the temporal resolution have to be refined for observers out of the rotation axis. Observing the relative error dependence on the angle θ, Fig. 9(b), confirms that the regions with maximum relative error are those where the acoustic pressures are minima. For some values of θ, $\overline{E}_r$ is nearly equal to 1, meaning that near the rotation axis, the error is significant. One could conclude that the large error shown in Fig. 9 at the rotation axis has no real significance in that the acoustic pressures at these locations are nearly zero as shown in Fig. 8(a). However, Fig. 8(b) illustrates that the acoustic pressure levels are not negligible in the rotation axis.

4. Tam test case

The second test case studied in this work has been presented by Tam [6] in the third CAA benchmark problems workshop. The problem consists of computing the noise radiated by a specified analytical force distribution. Subsequently, an exact solution [7] of the linearized Euler equations was developed for the first

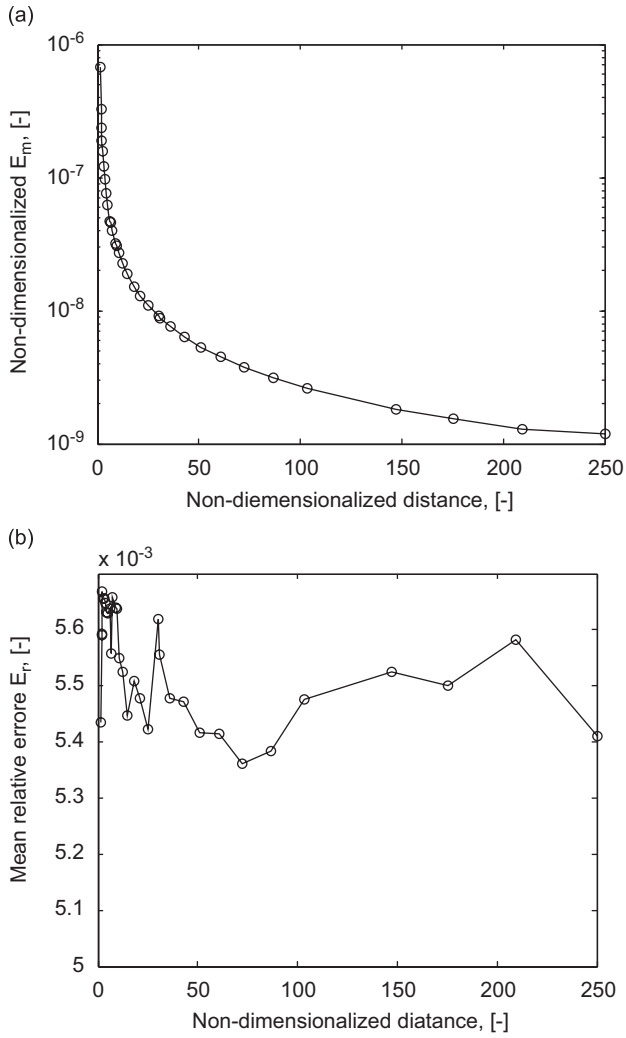

Fig. 7. Numerical errors as a function of source–observer distance, (a) error metric E_m, (b) mean relative error $\overline{E}_r$.

harmonic of the noise produced by this distribution of forces. The geometrical configuration is shown in Fig. 10: the rotor is 1.6 m long and its radius is 1 m.

In this section the variables are non-dimensionalized with respect to the following scales:

length scale	b, length of the blade
velocity scale	c_0, ambient sound speed
time scale	b/c_0
density scale	ρ_0, ambient fluid density
pressure scale	$\rho_0 c_0^2$
body force scale	$\rho_0 c_0^2/b$

The physical rotor is replaced in a cylindrical coordinates (x, r, φ) by the following distribution of forces:

$$\begin{bmatrix} F_r(r,\varphi,x,t) \\ F_\varphi(r,\varphi,x,t) \\ F_x(r,\varphi,x,t) \end{bmatrix} = \mathrm{Re}\left\{ \begin{matrix} 0 \\ \tilde{F}_\varphi(r,x) \\ \tilde{F}_x(r,x) \end{matrix} \right\} \mathrm{e}^{im(\varphi-\Omega t)} \tag{15}$$

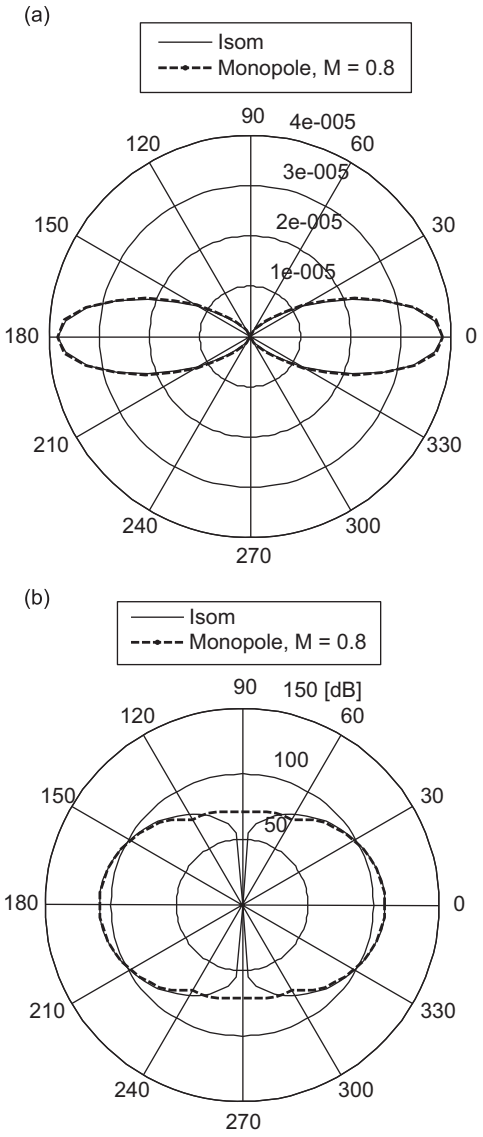

Fig. 8. Directivity of the maximum amplitude of the Isom and thickness noise $\max_{t=t_0}^{t=T}|\tilde{p}_T(t)|$ and $\max_{t=t_0}^{t=T}|\tilde{p}_L|$, respectively, (a) (Pa), (b) dB, $p_{ref} = 2 \times 10^{-5}$ Pa.

where

$$\tilde{F}_\varphi(r,x) = \begin{cases} F(x) r J_m(\lambda_{mN} r), & r \leqslant 1, \\ 0, & r > 1, \end{cases} \quad \tilde{F}_x(r,x) = \begin{cases} F(x) J_m(\lambda_{mN} r), & r \leqslant 1 \\ 0, & r > 1 \end{cases}$$

$$F(x) = \exp\{-(\ln 2)(10x)^2\}$$

and $J_m(\,)$ is the mth-order Bessel function, λ_{mN} is the Nth root of J'_m; i.e., $J'_m(\lambda_{mN}) = 0$. The calculation has been made for an eight blade rotor, so $m = 8$ and setting $N = 1$, the value of $\lambda_{mN} = 9.64742$. Ω is also non-dimensional.

Tam showed that the acoustic pressure for the sound radiated at the first harmonic $m\Omega$ can be approached by

$$\tilde{p}(R,\theta,t) \underset{R\to\infty}{\approx} \frac{2}{R} A(k_S) e^{im\Omega(R-t) - i/2(m+1)\pi} \tag{16}$$

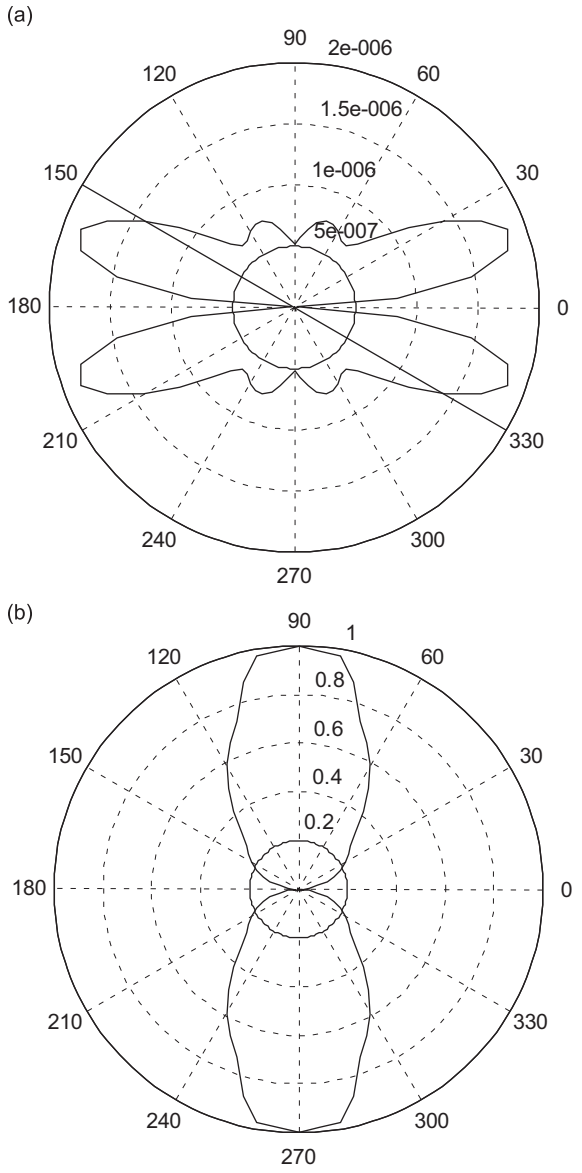

Fig. 9. Directivity of the numerical errors, (a) error metric E_m, (b) mean relative error $\overline{E}_r$.

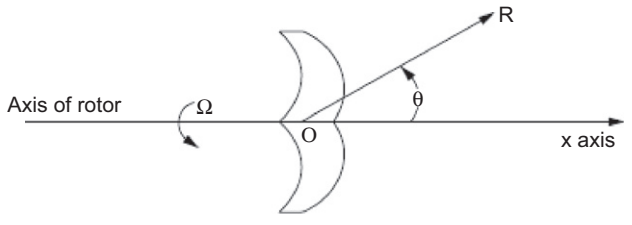

Fig. 10. Tam's open rotor.

where

$$A(k_S) = \frac{1}{4}\left(\frac{\pi}{100\ln 2}\right)^{1/2} \frac{m^2(1+\Omega\cos\theta)\Omega\sin\theta}{\lambda_{mN}^2 - m^2\Omega^2\sin^2\theta} J_m(\lambda_{mN}) J'_m(m\Omega\sin\theta) e^{-m^2\Omega^2\cos^2\theta/400\ln 2} \tag{17}$$

and $k_S = m\Omega\cos\theta$.

It is to be noted that the term $m\Omega\sin\theta$ in the expression for $A(k_s)$ presented in Eq. (17) appeared as $mR\sin\theta$ in Ref. [6]. This is certainly a typographical error. The directivity $D(\theta)$ in spherical coordinates is defined as

$$D(\theta) = \lim_{R\to\infty} R^2\overline{\tilde{p}^2(R,\theta,\varphi,t)} = 2A^2(k_S) \tag{18}$$

The over-bar denotes the time average. In order to test the code based on the FW&H equation, Tam's benchmark problem was adapted by Hirsch et al. [4,14] by removing the harmonic exponential dependence of the blade force. A new blade force was defined as

$$\begin{bmatrix} F_r(r,\varphi,x,t) \\ F_\varphi(r,\varphi,x,t) \\ F_x(r,\varphi,x,t) \end{bmatrix} = \mathrm{Re}\left\{ \begin{matrix} 0 \\ \tilde{F}_\varphi(r,x) \\ \tilde{F}_x(r,x) \end{matrix} \right\} \tag{19}$$

The aerodynamic forces defined in Eq. (19) are substituted into the loading noise sources of formulation 1A. The first harmonic of the computed solution should be identical to Tam's analytical solution. As the problem is axisymmetric about the x-axis the computational domain is defined in the r–x plane for $-0.8 \leqslant x \leqslant 0.8$ and $0 \leqslant r \leqslant 1$. The blade surface is discretized into equally spaced points (40 points along x-axis × 25 points along r-axis). The results given by Tam [6] are reproduced by the acoustic solver developed in this work.

Fig. 11 shows the results obtained for $\Omega = 0.85$ at $R = 100$ m. In Fig. 11(a) is shown the computed dipole far-field acoustic pressure with F1A at ($\theta = 90^\circ$ and $R = 100$ m, $\Omega = 0.85$). The first harmonic of this signal is compared to Tam's analytical solution in Fig. 11(b). The computed directivity of the first harmonic is presented in Fig. 11(c). The results agree perfectly. This suggests that the numerical method predicts the dipole noise accurately at $\Omega = 0.85$. The same results are presented in Fig. 12 for $\Omega = 0.6$. Some discrepancies are noticed and the agreement is less significant. These results reinforce those obtained in the Mach number effect study for Isom's test case.

5. Conclusion

Development of the Ffowcs Williams and Hawkings equation is carried out. The acoustic solver is based on the integral retarded time of formulation 1A developed by Brentner and Farassat. The retarded-time integrals are approximated by a mid-panel-quadrature algorithm. They are calculated with the source time regarded as the primary time (i.e., dominant). The second and then the fourth-order equidistant derivations are used for the evaluation of aerodynamic loadings. An interpolation of the acoustic pressure at the reception time is performed with linear, spline or piecewise cubic Hermite interpolating polynomial so that the contributions from all source panels are summed at the same observer times.

A parametric study of the relevant criteria is conducted based on Isom's and Tam's test cases. In order to compare the results obtained when parameters are varied, error metric and relative average error definitions are introduced. For Isom's test case, thickness noise is compared to loading noise whereas, for Tam's benchmark, the comparison is performed between analytical and numerical solutions.

The same helicopter rotor, as defined by Farassat to study Isom's case, is used. The mean relative error decreases when the Mach number increases. This result suggests that the mesh must be refined near the regions moving at low Mach number. Although the errors decrease when temporal resolution is refined, the results are very sensitive to interpolation algorithm type. The spline interpolation is giving the best accuracy for low temporal resolution. However, all algorithms tend to the same accuracy for high temporal resolution. For the configuration presented, 512 time steps are sufficient to give a minimum error. For practical configurations, conducting this test should give the minimum number of time steps needed to have an accurate acoustic solution.

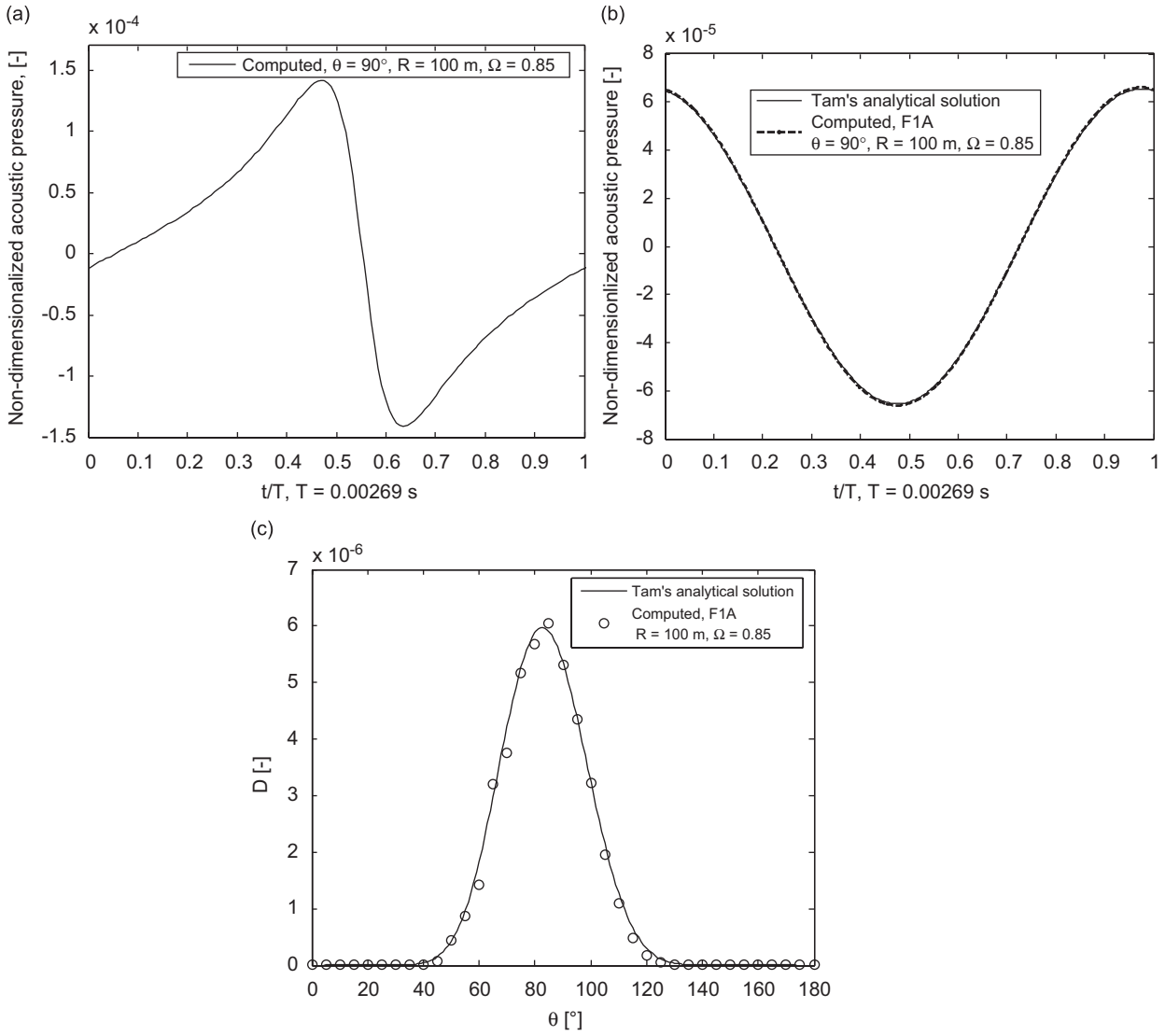

Fig. 11. Acoustic results for $\Omega = 0.85$: (a) computed dipole acoustic pressure with F1A, (b) computed first harmonic signal with F1A compared to Tam's analytical solution, Eq. (15), (c) computed first harmonic directivity with F1A compared to Tam's analytical solution, Eq. (17).

Even if, theoretically, the formulation F1A is adequate to predict the near-field aerodynamic noise, the numerical results are sensitive to source–observer distance. The absolute error decreases when the observer is in the far field. However, the discrepancy between loading noise and thickness noise is nearly constant in relative value. In other terms, the far-field and near-field integrals are estimated with the same accuracy.

The directivity feature shows a dipole character. The acoustic pressures found are maxima in the rotation plane. On the other hand, the acoustic pressures are minima along the rotation axis. This is explained by the fact that on the rotation axis, the tangential forces are not responsible for noise emission (source terms L_r are null for this force components since the tangential forces are perpendicular to the source–observer vector $\mathbf{r}$). Only axial forces can generate noise on the rotation axis.

The analysis is then extended to Tam's test case. The results agree in case of $\Omega = 0.85$, whereas, for $\Omega = 0.6$, some discrepancies are noticed confirming that the errors increase when tip Mach number decreases.

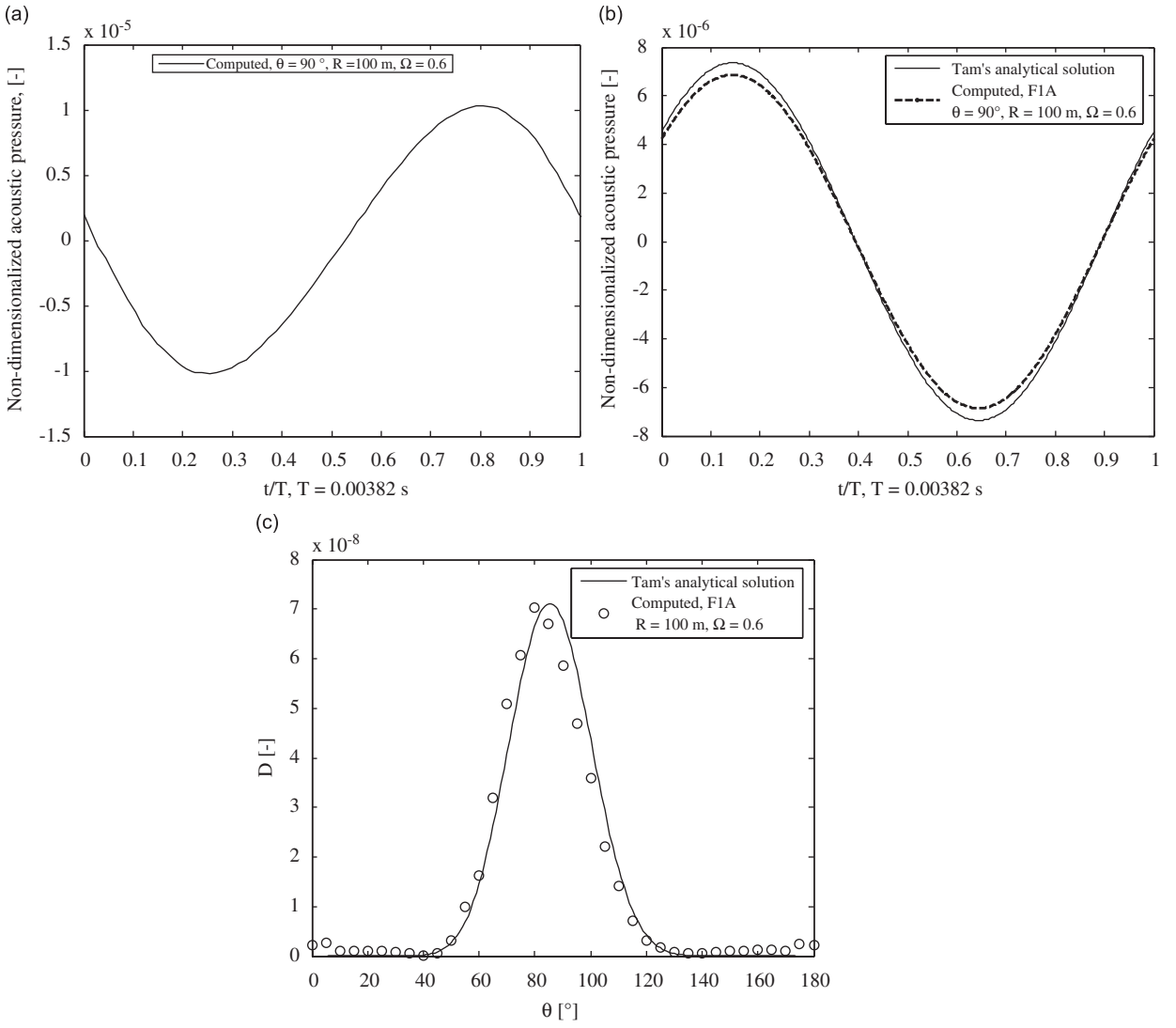

Fig. 12. Acoustic results for $\Omega = 0.85$: (a) computed dipole acoustic pressure with F1A, (b) computed first harmonic signal with F1A compared to Tam's analytical solution, (c) computed first harmonic directivity with F1A compared to Tam's analytical solution.

Acknowledgment

The authors would like to thank Pr. Hirsch for suggesting the Isom thickness case as a verification base. They would like to thank Pr. Gary W. Rankin for his reading and discussing of the paper.

Appendix A

The central difference formula for the second-order temporal derivation is given as

$$\left(\frac{\partial \Phi}{\partial \tau}\right)_n = \frac{\Phi_{n+1} - \Phi_{n-1}}{2\Delta\tau}$$

The fourth-order temporal derivation is calculated through a five point central difference formula:

$$\left(\frac{\partial \Phi}{\partial \tau}\right)_n = \frac{\Phi_{n-2} - 8\Phi_{n-1} + 8\Phi_{n+1} - \Phi_{n+2}}{12\Delta\tau}$$

When the retarded time steps are non-equidistant, the second-order derivation has the form

$$\left(\frac{\partial \Phi}{\partial \tau}\right)_n = \frac{(\tau_n - \tau_{i-1})^2\Phi_i - (\tau_i - \tau_n)^2\Phi_{i-1}}{(\tau_i - \tau_n)(\tau_n - \tau_{i-1})(\tau_i - \tau_{i-1})} + \frac{[(\tau_n - \tau_i)^2 - (\tau_i - \tau_{i-1})^2]\Phi_n}{(\tau_i - \tau_n)(\tau_n - \tau_{i-1})(\tau_i - \tau_{i-1})}$$

where

$\Phi(\tau_n) = \Phi(\tau_i)\tau_n - \tau_{i-1}/\tau_i - \tau_{i-1} + \Phi(\tau_{i-1})\tau_i - \tau_n/\tau_i - \tau_{i-1}$, τ_i is the first time $\tau_i \leqslant \tau_n$ where the aerodynamic data are available.

The fourth-order temporal derivation could be calculated through the polynomial development as follows:

$$\left(\frac{\partial \Phi}{\partial \tau}\right)_n = a_1 + 2a_2\tau_n + 3a_3\tau_n^2$$

where

$$a_i = \frac{\Delta_i}{\Delta}$$

$$\Delta = \begin{vmatrix} 1 & \tau_{i-1} & \tau_{i-1}^2 & \tau_{i-1}^3 \\ 1 & \tau_i & \tau_i^2 & \tau_i^3 \\ 1 & \tau_{i+1} & \tau_{i+1}^2 & \tau_{i+1}^3 \\ 1 & \tau_{i+2} & \tau_{i+2}^2 & \tau_{i+2}^3 \end{vmatrix} = 12(\Delta\tau)^6$$

$$\begin{aligned} \Delta_1 &= \begin{vmatrix} 1 & \Phi_{i-1} & \tau_{i-1}^2 & \tau_{i-1}^3 \\ 1 & \Phi_i & \tau_i^2 & \tau_i^3 \\ 1 & \Phi_{i+1} & \tau_{i+1}^2 & \tau_{i+1}^3 \\ 1 & \Phi_{i+2} & \tau_{i+2}^2 & \tau_{i+2}^3 \end{vmatrix} \\ &= -2(\Delta\tau)^3[3\tau_i^2 + 6\tau_i\Delta\tau + 2(\Delta\tau)^2]\Phi_{i-1} + 6(\Delta\tau)^3[3\tau_i^2 + 4\tau_i\Delta\tau + 2(\Delta\tau)^2]\Phi_i \\ &\quad - 6(\Delta\tau)^3[3\tau_i^2 + 4\tau_i\Delta\tau + 2(\Delta\tau)^2]\Phi_{i+1} + 2(\Delta\tau)^3[3\tau_i^2 + (\Delta\tau)^2]\Phi_{i+2} \end{aligned}$$

$$\begin{aligned} \Delta_2 &= \begin{vmatrix} 1 & \tau_{i-1} & \Phi_{i-1} & \tau_{i-1}^3 \\ 1 & \tau_i & \Phi_i & \tau_i^3 \\ 1 & \tau_{i+1} & \Phi_{i+1} & \tau_{i+1}^3 \\ 1 & \tau_{i+2} & \Phi_{i+2} & \tau_{i+2}^3 \end{vmatrix} \\ &= 6(\Delta\tau)^3[\tau_i + \Delta\tau]\Phi_{i-1} - 6(\Delta\tau)^3[3\tau_i + 2\Delta\tau]\Phi_i \\ &\quad + 6(\Delta\tau)^3[3\tau_i + \Delta\tau]\Phi_{i+1} - 6(\Delta\tau)^3\tau_i\Phi_{i+2} \end{aligned}$$

$$\Delta_3 = \begin{vmatrix} 1 & \tau_{i-1} & \tau_{i-1}^2 & \Phi_{i-1} \\ 1 & \tau_i & \tau_i^2 & \Phi_i \\ 1 & \tau_{i+1} & \tau_{i+1}^2 & \Phi_{i+1} \\ 1 & \tau_{i+2} & \tau_{i+2}^2 & \Phi_{i+2} \end{vmatrix}$$

$$= -2(\Delta\tau)^3\Phi_{i-1} + 6(\Delta\tau)^3\Phi_i + 6(\Delta\tau)^3\Phi_{i+1} - 2(\Delta\tau)^3\Phi_{i+2}$$

References

[1] F. Farassat, G.P. Succi, The prediction of helicopter discrete frequency noise, *Vertica* 7 (4) (1983) 309–320.

[2] P. Di Francescantonio, A new boundary integral formulation for the prediction of sound radiation, *Journal of Sound and Vibration* 202 (4) (1997) 491–509.

[3] D. Casalino, An advanced time approach for aeroacoustic analogy predictions, *Journal of Sound and Vibration* 261 (2003) 583–612.

[4] G. Ghorbaniasl, C. Hirsch, Validation and application of a far-field time domain formulation for fan noise prediction, *11th AIAA/CEAS Aeroacoustics Conference*, AIAA 2005-2838.

[5] M.P. Isom, *The Theory of Sound Radiated by a Hovering Transonic Helicopter Blade*, Poly-AE/AM, No. 75-4, Polytechnic Institute of New York, 1975.

[6] C. Tam, Rotor noise: category 2, benchmark problems, *Third Computational Aeroacoustics (CAA) Workshop on Benchmark Problems*, 2000, NASA/CP-2000-209790.

[7] C. Tam, Rotor noise: category 2, analytical solution, *Third Computational Aeroacoustics (CAA) Workshop on Benchmark Problems*, 2000 NASA/CP-2000-209790.

[8] J.E. Ffowcs Williams, D.L. Hawkings, Sound generated by turbulence and surfaces in arbitrary motion, *Philosophical Transactions of the Royal Society A* 264 (1969) 321–342.

[9] K.S. Brentner, F. Farassat, Modeling aerodynamically generated sound of helicopter rotors, *Progress in Aerospace Sciences* 39 (2003) 83–120.

[10] F. Farassat, The derivation of a thickness noise formula for the far-field by Isom, *Journal of Sound and Vibrations* 64 (1) (1979) 159–160.

[11] F. Farassat, Extension of Isom's thickness noise formula to the near field, *Journal of Sound and Vibrations* 67 (2) (1979) 280–281.

[12] F. Farassat, Isom's thickness noise formula for rotating blades with finite thickness at the tip, *Journal of Sound and Vibrations* 72 (4) (1980) 550–553.

[13] F. Farassat, R. Martin, A note on the tip noise of rotating blades, *Journal of Sound and Vibrations* 86 (3) (1983) 449–453.

[14] Ch. Hirsch, Gh. Ghorbaniasl, J. Ramboer, Fan noise simulation in the time domain: validation test cases, *The Second International Symposium on Fan Noise*, Senlis, France, 2003.